Article

Rhodium Catalyst Structural Changes during, and Their Impacts on the Kinetics of, CO Oxidation

Silvia Marino, Lai Wei, Marina Cortes-Reyes, Yisun Cheng, Paul Laing, Giovanni Cavataio, Christopher Paolucci, and William Epling*

Read Online

| ACCESS | | Metrics & More | | Article Recommendations | | Supporting Information |

ABSTRACT: Catalysts can undergo structural changes during the reaction, affecting the number and/or the shape of active sites. For example, Rh can undergo interconversion between nanoparticles and single atoms when CO is present in the reaction mixture. Therefore, calculating a turnover frequency in such cases can be challenging as the number of active sites can change depending on the reaction conditions. Here, we use CO oxidation kinetics to track Rh structural changes occurring during the reaction. The apparent activation energy, considering the nanoparticles as the active sites, was constant in different temperature regimes. However, in a stoichiometric excess of O_2, there were observed changes in the pre-exponential factor, which we link to changes in the number of active Rh sites. An excess of O_2 enhanced CO-induced Rh nanoparticle disintegration into single atoms, affecting catalyst activity. The temperature at which these structural changes occur depend on Rh particle size,

with small particle sizes disintegrating at higher temperature, relative to the temperature required to break apart bigger particles. Rh structural changes were also observed during in situ infrared spectroscopic studies. Combining CO oxidation kinetics and spectroscopic studies allowed us to calculate the turnover frequency before and after nanoparticle redispersion into single atoms.

KEYWORDS: heterogeneous catalysis, dynamic catalysis, Rh, single atom catalysis, CO oxidation kinetics
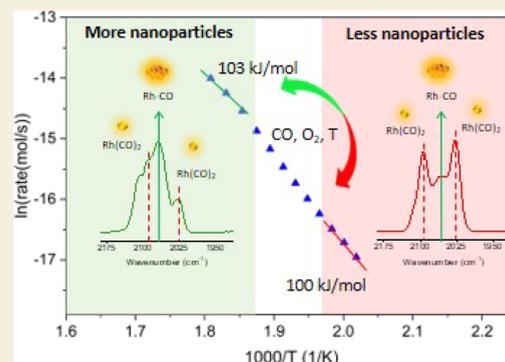
INTRODUCTION

It is becoming more recognized that catalyst structure can be dynamic, changing with time on stream and reactor and reaction conditions.[1−6] These catalyst structural changes can alter the catalyst activity and the selectivity toward desired products.[7,8] Of course, they can also complicate kinetic analysis due to site type and density changes. Therefore, studying catalyst dynamics under reaction conditions is critical in understanding reactions, mechanisms, and designing catalysts.

There are several literature studies that demonstrate reductant or oxidant-induced mobility of catalytically active sites. Structural evolution of single atoms to nanoparticles with exposure to high temperature reducing treatments has been widely reported for Pt and Pd supported on oxide supports and zeolites.[9−12] These structural changes can also be reversible with fragmentation of nanoparticles into isolated single atoms occurring when the catalyst is exposed to oxidizing conditions and high temperature.[13,14]

In some cases, adsorbate-induced structural changes have been observed under reaction conditions. Pt restructuring was observed via infrared (IR) spectroscopy during CO oxidation, where the fraction of well-coordinated and under-coordinated sites changed.[15] Operando electron microscopy was used to track unsupported Pd nanoparticle structural changes as a function of temperature during CO oxidation. At low

temperature, Pd nanoparticles would present low index planes that showed low activity toward CO oxidation, while at high temperature, the nanoparticles assumed a rounder surface leading to a higher CO conversion.[16] Theoretical studies combined with X-ray absorption experiments showed that in the presence of NH_3, Cu ions become solvated by NH_3 and mobile, enabling them to combine and form ion pairs that participate in the selective catalytic reduction redox cycle.[17,18] Pd nanoparticles' disintegration into single atoms on Pd/Al_2O_3 was observed during methane oxidation in an excess of O_2. Pd nanoparticle redispersion caused by the oxidative environment led to the loss of active sites and therefore to lower activity.[19] In all these cases, the number of active sites changed when the catalysts were exposed to the reaction mixture.

Here, we focus on Rh structural changes occurring during CO oxidation. Changes in the Rh particle distribution have been widely reported.[11,20−31] These changes have been characterized using diffuse reflectance infrared Fourier trans-

form spectroscopy (DRIFTS),[20,28,30,32−34] temperature-programed reduction,[35] extended X-ray absorption spectroscopy,[34−37] scanning tunnel microscopy (STM),[38] scanning transmission electron microscopy,[39] nuclear magnetic resonance,[40] and X-ray photoelectron spectroscopy[41] and predicted in theoretical studies.[4,42,43] At low temperature, CO breaks apart Rh nanoparticles, dispersing them into single atoms. One proposed mechanism suggests that the bond energy between CO and Rh overcomes the Rh−Rh and Rh-support bond energies, favoring nanoparticle disintegration.[34,37,44] Other studies have proposed that Rh particle disintegration involves an oxidative process where the Rh-oxidation state changes from 0 to +1 with the assistance of OH groups on the support.[20,21,45] CO-induced Rh particle disintegration can be reversible, for example, STM imaging and IR spectroscopy experiments show that Rh single atoms re-aggregate into nanoparticles during CO exposure at high temperature.[38] With structural changes occurring during the reaction, when CO is present, the number of active sites may change, affecting the activity of the reaction. As a consequence, counting active sites via ex situ measurements may not provide an accurate representation of the system under study and can lead to an incorrect calculation of the turnover frequency. Indeed, some previous studies have used the rates of CO oxidation as a probe reaction to estimate the active metal surface area since its reaction kinetics on Pt-group metals (PGMs) is well known.[46,47]

CO oxidation is likely the most studied reaction in heterogeneous catalysis and has been often used to answer mechanistic and catalyst structural questions due to its relative simplicity.[48,49] However, in the case of CO oxidation on Rh catalysts, due to CO-induced Rh structural changes, quantifying the number of active sites and therefore turnover frequency when CO is a reactant or intermediate is challenging. Furthermore, a better understanding of the active site's dynamics during Rh restructuring under reaction conditions and its consequences on catalyst activity would allow catalyst design optimization, which is critical in light of the recent volatility in Rh price.

Here, we monitored kinetic parameters, specifically the activation energy and pre-exponential factor, to identify when structural changes occurred during the reaction. We found that under conditions with a stoichiometric excess of oxygen, Rh nanoparticles are readily dispersed into single atoms and that the temperature at which dispersion occurs depends on the initial Rh particle size. CO-induced nanoparticle disintegration in the presence of an excess of O_2 was also observed using DRIFTS. The concentration of oxygen in the gas mixture affects the extent of particle dispersion caused by CO. Combining kinetic and spectroscopic studies, we were able to quantify the extent of particle disintegration and calculate the turnover frequency.

■ MATERIALS AND METHODS

Catalysts

A series of Rh/Al_2O_3 catalysts were synthesized using the incipient wetness method. $Rh(NO_3)_3$ was used as the precursor, with the rhodium(III) nitrate solution (10% w/w Rh in >5 wt % HNO_3 solution) purchased from Sigma-Aldrich, and was deposited onto γ-Al_2O_3, also purchased from Sigma-Aldrich, to achieve 0.05 and 0.1% Rh weight loadings. The Rh-containing catalysts were dried in a Thermo Scientific Lindberg muffle furnace at 120 °C for 4 h in static air, and then the temperature was ramped to 600 °C at 1 °C/min and

held there for 4 h. To obtain different particle sizes, different samples were placed in a quartz tube, which was put inside a Lindberg Blue M tube furnace purchased from Thermo Scientific and exposed to 5% H_2 in N_2 at 700 °C for 4 h, 800 °C for 4 h, or 900 °C for 72 h. Another 0.1 wt % Rh/Al_2O_3 catalyst provided by the Ford Motor Company was also evaluated as part of this study; to demonstrate that the approach should be extrapolatable as different alumina supports, including a commercial support, precursors and pretreatment methods were used in its synthesis. This sample was synthesized by wetness impregnation using a $Rh(NO_3)_3$ (10% w/w in 20−25% HNO_3 solution) precursor, purchased from Acros Organics, deposited onto γ-Al_2O_3 (Puralox Sasol). The catalyst was calcined at 500 °C for 8 h. The catalyst was then aged following Ford's 4-mode aging protocol[50] to simulate the performance of a high-mileage catalyst. This sample is referred to as "Cycling Aged" below.

Chemisorption

H_2 chemisorption was performed using a Micromeritics ASAP2020 Plus. The amount of sample used ranged from 700 to 900 mg, and the samples were characterized after synthesis with no further treatments prior to being placed in the chemisorption unit. Prior to the measurements, the catalysts were reduced in H_2 at 500 °C for 1 h, then evacuated for 2 h at 500 °C, cooled to 35 °C, and maintained under vacuum for 1 h. The H_2 adsorption isotherms were collected at 35 °C. The dispersion was calculated assuming a H/metal ratio = 1:1. We used the inverse of dispersion to calculate the average particle size, assuming hemispherical clusters. Measured values are shown in Table S1.

CO Oxidation Kinetic Experiments

The catalyst was placed in a quartz tube having an internal diameter of 4 mm. The tube was placed in a Thermo Scientific Lindberg Blue M tube furnace. The inlet and outlet temperatures were measured using K-type thermocouples purchased from Omega. Inlet and outlet stainless steel tubing was maintained at 150 °C to avoid water condensation. The amount of catalyst used was 5−13 mg. In order to avoid heat transfer limitations, the catalyst was diluted with crushed cordierite, originating from a Corning cordierite monolith, with a catalyst/cordierite weight ratio varying between 1:18 and 50. Cordierite is a common support material for monolith-supported catalysts and typical in automotive catalysis.[51] The cordierite inactivity during the reaction was confirmed, with the results shown in Figure S1. To avoid internal diffusion limitations, the catalysts were pelletized and sieved to obtain 80−170 mesh (0.177−0.088 mm) pellets. The flowrates used were between 500 and 750 sccm, which according to our calculations is enough to avoid external mass transfer limitations. The absence of these transport limitations at conversions typically below 20% was confirmed using the Weisz−Prater number[52] and the Anderson and Mear's criteria.[53,54] N_2, CO, O_2, and H_2 flowrates were controlled with MKS mass flow controllers. Experiments that included H_2O were also performed, with 6% H_2O, using a Bronkhorst-controlled evaporator mixer. The catalysts were pretreated in 5% H_2 in N_2 at 500 °C for 30 min. CO oxidation experiments were performed using CO concentrations between 8400 and 13,000 ppm. The O_2 concentration was adjusted to maintain a target CO/O_2 ratio. CO, CO_2, and H_2O concentrations were measured using a MKS MG2030 Fourier transform infrared (FT-IR) analyzer. The conversions shown in the figures were obtained under steady-state conditions, with decreasing reaction temperature between data points.

DRIFTS Experiments

DRIFTS experiments were performed using a Nicolet iS50 FT-IR, with the adsorption of CO to characterize Rh speciation. The flowrate used for the pretreatments and experiments was 50 sccm. The pretreatment consisted of exposure to 1% O_2 in He at 500 °C for 30 min, followed by a 10 min He purge, with a final exposure to 5% H_2 in N_2 at 500 °C for 30 min. The temperature was then decreased in He to 35 °C. The catalysts were exposed to 8400 ppm of CO in 16% N_2 and 83% He until saturation, which was verified by the unchanging spectra.

DRIFTS experiments with the goal of simulating reactor experiments were performed using the 0.1 wt % Rh/Al$_2$O$_3$ sample that had been treated in H$_2$ at 700 °C as described above, using a custom-made split cell design purchased from Harrick Scientific. The cell includes two sample holders, one for the catalyst and the other for a reference material. The chamber is mounted on a movable stage that allows us to switch between characterizing the catalyst and the reference. Half of the cell was loaded with the catalyst and the other half with inert SiC. This split cell design allowed us to subtract the gas-phase spectrum, obtained when collecting the IR signal from the inert material side, from the spectrum obtained when collecting from the catalyst side, at each temperature. The catalyst underwent the pretreatment protocol described above and was then cooled to 300 °C in He. Prior to the experiments, the background spectra for the catalyst and SiC were taken at each temperature in He. The catalysts were exposed to a gas mixture containing 8400 ppm CO and 9250 ppm O$_2$ diluted in 16% N$_2$ and 82% He, and the species present on the catalyst surface were analyzed every 20 °C between 300 and 220 °C. The gas-phase subtraction was performed using absorbance as intensity units. In the plots shown, the spectra have been converted into Kubelka—Munk units.

■ RESULTS AND DISCUSSION

Catalyst Characterization: H$_2$ Chemisorption and CO DRIFTS

Samples with a range of Rh particle sizes were synthesized by varying the Rh loading and the H$_2$ reduction temperature, with Table 1 listing the particle size measurements obtained using

Table 1. Average Particle Sizes Measured via H$_2$ Chemisorption

catalyst	average particle size [nm]
0.05%Rh/Al$_2$O$_3$	<1
0.1%Rh/Al$_2$O$_3$	1.1
0.1%Rh/Al$_2$O$_3$ H$_2$-700°C	1.6
0.1%Rh/Al$_2$O$_3$ H$_2$-800°C	3.3
0.1%Rh/Al$_2$O$_3$-Cycling Aged	5
0.1%Rh/Al$_2$O$_3$ H$_2$-900°C-72 h	9.2

H$_2$ chemisorption and Table S1 listing the dispersion values. The values obtained from the H$_2$ chemisorption experiments correspond to average values. A separate sample was synthesized and aged at high temperature with exposure to oxidizing and reducing conditions,[66] which is labeled "Cycling Aged" in later results and is included to demonstrate that the trends observed extrapolate beyond those samples exposed to simpler conditions and synthesized with a different alumina and precursor. CO DRIFTS has been used to characterize Rh speciation, enabling the identification of Rh-oxidation states as well as distinguishing between single atoms, via the presence of Rh *gem*-dicarbonyls, and Rh nanoparticles.[20,21,24,30,55,56] To characterize our samples, CO adsorption spectra were obtained after reducing the catalysts in H$_2$ at 500 °C, Figure 1. The spectra contain three main features at 2030, 2060, and 2100 cm^{-1}. The features at 2100 and 2030 cm^{-1} correspond to the IR symmetric and asymmetric stretches of a single atom Rh as a *gem*-dicarbonyl [Rh$^+$(CO)$_2$], respectively. The feature between 2040 and 2070 cm^{-1} corresponds to CO linearly bound to Rh nanoparticles,[22,30,55] displayed as Rh^0–CO. The Rh^0–CO peak position depends on the particle size, CO coverage, and local coordination environment.[22,57–60] For the catalysts with particle sizes 3.3 nm or larger, as was calculated from the H$_2$ chemisorption results, there was also a small feature in the 1800–1900 cm^{-1} range, indicating the presence
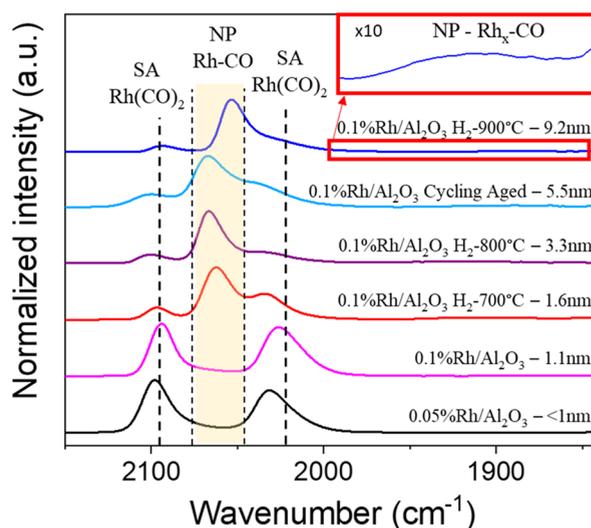
Figure 1. DRIFTS spectra obtained after a He purge, which followed CO adsorption at 35 °C on 0.05%Rh/Al$_2$O$_3$, 0.1%Rh/Al$_2$O$_3$, 0.1% Rh/Al$_2$O$_3$H$_2$-700 °C, 0.1%Rh/Al$_2$O$_3$H$_2$-800 °C, 0.1%Rh/Al$_2$O$_3$-Cycling-Aged, and 0.1%Rh/Al$_2$O$_3$ H$_2$-900 °C—plotted in rank of dispersion as measured by H$_2$ chemisorption. The CO concentration during the exposure was 8400 ppm. Prior to CO adsorption, the catalysts were reduced at 500 °C in 5% H$_2$ for 30 min. The Kubelka—Munk intensity of the largest peak in each spectrum was normalized to 1. For the 0.1%Rh/Al$_2$O$_3$ H$_2$-900 °C sample, the KM intensity between 1950 and 1840 cm^{-1} was multiplied by 10 and displayed in the inset red-bordered box.

of bridge-bound CO on Rh nanoparticles (Rh$_x$–CO). An example is shown in the inset for the 0.1% Rh sample aged at 900 °C for 72 h. Overall, with increasing dispersion, there are more Rh(CO)$_2$ single atoms relative to nanoparticles. This increased Rh(CO)$_2$ amount relative to nanoparticles might simply be due to the lower reduction temperature used in synthesis or the lower Rh loading, both of which would normally lead to less metal agglomeration. However, it is widely reported that at low temperature, CO is able to break apart Rh particles, dispersing them into single atoms, and that the relative fraction of Rh single atoms and nanoparticles formed during CO exposure at low temperature changes as a function of particle size.[20–22,29,30,55,56] We hypothesize that CO exposure at 35 °C during the DRIFTS experiment led to an increase in the Rh(CO)$_2$ amount relative to nanoparticles.

CO Oxidation Kinetics

CO oxidation is one of the most studied reactions in heterogeneous catalysis, and the generally accepted active site for PGM on irreducible oxide supports is the metallic phase, when the reaction is performed under stoichiometric or slightly oxidizing conditions.[56,61–67] Since it is so well studied, and often used as a probe reaction, calculating turnover frequencies is needed, and to do so for Rh-supported catalysts, we need to understand how the number of active sites changes under reaction conditions. Here, we use CO oxidation rates to understand when the number of active sites changes under reaction conditions and, ultimately, in combination with spectroscopy to calculate turnover frequencies.

Figure 2 shows the Arrhenius plots originating from the experiments using the 0.05%Rh/Al$_2$O$_3$, 0.1%Rh/Al$_2$O$_3$ H$_2$-700 °C, and 0.1%Rh/Al$_2$O$_3$ H$_2$-900 °C catalysts. Results from the rest of the samples are shown in Figure S2. These catalysts have initial average Rh particle sizes that span from <1 to 9.2
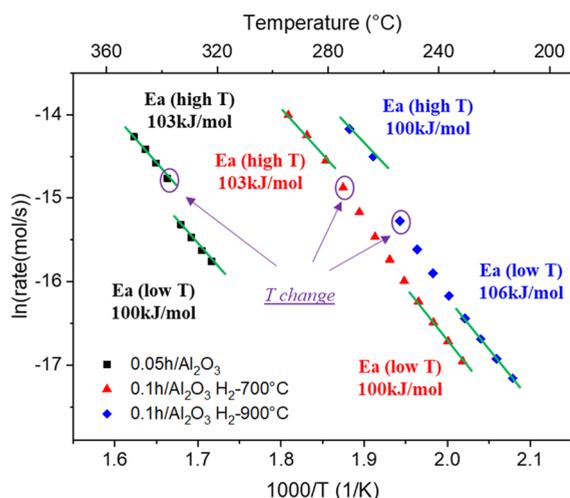
Figure 2. CO oxidation Arrhenius plots obtained from the 0.05%Rh/Al_2O_3, 0.1%Rh/Al_2O_3 H_2-700 °C, and 0.1%Rh/Al_2O_3 H_2-900 °C samples. CO = 8400−13,000 ppm, CO/O_2 = 0.9, total flowrate = 500−750 sccm. The catalysts were pretreated in 5% H_2 at 500 °C for 30 min. The results shown were obtained after reaching steady state, with the experiment run from high to low temperature.

nm. Results are shown from an experiment with decreasing temperature; however, similar results were obtained with increasing temperature. In the Arrhenius plots in Figure 2, we expressed the rate in mol/s of CO_2 formed. We refrained from normalizing them by the moles of surface Rh measured via H_2 chemisorption, due to the redistribution of Rh speciation and/or structure that occurs in the presence of CO, as hinted at from the CO DRIFTS spectra in Figure 1 and the literature discussed in the Introduction section. CO-induced particle restructuring makes the number of active sites unknown under reaction conditions as the number of active sites will be different from that obtained from H_2 chemisorption or other ex situ measurements.

All the three Arrhenius plots in Figure 2 show the presence of multiple regimes. At low temperature, for all the three catalysts described in Figure 2, and for all the catalysts tested (Figure S2), the apparent activation energies are 100−110 kJ/mol. This is consistent with Langmuir−Hinshelwood-type kinetics previously reported, which involves the adsorption of CO and O_2, the dissociation of O_2, and a surface reaction forming CO_2.[68−72] At low temperature, the metal surface is covered by CO, resulting in reaction inhibition. CO has to desorb in order to allow O_2 to adsorb and dissociate.[46,72,73] As a consequence, the step limiting the reaction is the desorption of CO from the metal. The CO oxidation activation energy is similar to the CO desorption energy, consistent with our results.[66]

In the middle temperature range, for all but the smallest particle sizes, there is an observed increase in Arrhenius plot slopes as the measured reaction rates deviate from the linear fitting extrapolated from the low-temperature regime. The reason for this slope change is discussed below. At high temperature, the calculated apparent activation energies are once again 100−110 kJ/mol, similar to the values calculated in the low-temperature regime. These results suggest that the rate-limiting step at high and low temperature is the same and that the apparent activation energies in both temperature ranges correspond to the CO desorption energy from a Rh metal particle.[66] It is worth emphasizing that the heat and mass

transfer phenomena were negligible under these conditions—as mentioned in the Materials and Methods section, the absence of heat and mass transfer limitations was confirmed by calculating the Mear's and Anderson criteria and the Weisz−Prater number, all of which are further described in the Supporting Information, Section 4. The increase in the slope in the mid-temperature range for most of the samples or consistency between the low- and high-temperature ranges further excludes the presence of mass transfer limitations.

Although the apparent activation energies obtained for all the catalysts in the low- and high-temperature regimes are similar, the derived linear fitting for each pair of temperature regimes do not show the same y-intercept. Therefore, the pre-exponential factor differs between the high- and low-temperature regimes and is higher in the high-temperature regime. With the pre-exponential factor being a function of the number of active sites, these data suggest that the number of active sites changed between the low- and high-temperature regimes. As previously mentioned, at low temperature, CO is able to disperse Rh nanoparticles into single atoms, which leads to a decrease in the number of active sites for CO oxidation.[74] This is consistent with our results as the catalysts show lower pre-exponential factors at low temperature. However, with increasing temperature, the isolated single atoms reaggregate into nanoparticles in the presence of CO,[36,38] increasing the number of active sites for CO oxidation and thus the pre-exponential factor.

For the samples with average particle sizes of 1.6 and 9.2 nm, there are data points in the transition, or mid-temperature regime, between the low- and high-temperature regimes where the activation energies are consistent with known CO oxidation kinetics. In this transition temperature region, the Arrhenius plot slopes cannot be used to calculate an activation energy because the number of active sites is different for each data point. Therefore, a calculated higher "activation energy" in this transition does not represent a different rate-liming step but simply reflects changes in rate due to changes in the number of active sites as we move to higher temperature. It is possible to use these data to identify the pre-exponential factor and thus the number of, or change in, active sites. If the activation energy calculated from the low- and high-temperature regimes are assumed to be constant, then a similar Arrhenius-type line can be drawn through the rate point in the intermediate temperature regime and its y-intercept used to estimate the pre-exponential factor. The presence of a transition regime suggests that there might be a particle size distribution, with the smaller particles dispersing to single atoms before the larger as we decrease temperature, resulting in a decreased rate, until all the particles that will break apart do. However, the 0.05%Rh/Al_2O_3 catalyst does not show this intermediate/transition regime. Based on our interpretation of particle disruption or agglomeration being a function of particle size, this lack of a transition regime we speculate is due to particle sizes being relatively uniform such that they all disperse into single atoms between two experimental temperature points.

The temperatures at which the Arrhenius plot slopes change in Figure 2 show a particle size dependence. Figure 3 summarizes the temperatures at which we start to see a deviation from the linear fitting in the high-temperature region of the Arrhenius plots, which we here refer to as *T change*, for all the catalysts we studied. This *T change* value initially decreases with increasing particle size, reaching a plateau for
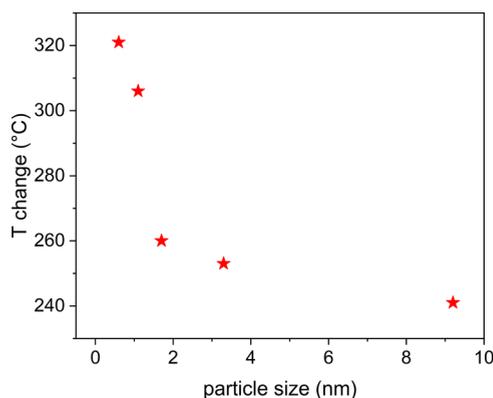
Figure 3. Summary of the temperature at which the change in CO oxidation kinetics occurs for 0.05%Rh/Al$_2$O$_3$ (<1 nm), 0.1%Rh/Al$_2$O$_3$ (1.1 nm), 0.1%Rh/Al$_2$O$_3$H$_2$-700 °C (1.6 nm), 0.1%Rh/Al$_2$O$_3$H$_2$-800 °C (3.3 nm), and 0.1%Rh/Al$_2$O$_3$H$_2$-900 °C (9.2 nm). CO = 8400−13,000 ppm, CO/O$_2$ = 0.9, flowrate = 500−750 sccm. The catalysts were pretreated in 5% H$_2$ at 500 °C for 30 min. The cycle-aged sample result is included in Figure S7.

samples with initial Rh particle sizes larger than 5 nm. Going from high to low temperature, smaller particles break apart into single atoms before larger particles. A particle size dependence is consistent with previously reported computationally predicted behavior of CO-induced disruption of Rh particles, where small particles in the presence of CO have a lower free energy of disintegration, leading to fragmentation to single atoms, while larger particles are more difficult to disintegrate.[42,43]

The inclusion of water, which is commonly present in many reactions, either as a reactant or a product, was investigated during CO oxidation to evaluate if similar phenomena can be observed. As shown and discussed in the Supporting Information (Section 5), water does not affect the CO oxidation mechanism because the measured apparent activation energies again correspond to the CO desorption energy, similar to the case without water. In addition, the presence of water did not alter the observed changes in the slope and the *T change* remained unchanged, see Figure S5 for example, suggesting that the interconversion between single atoms and nanoparticles is not affected.

Once the *T change* temperature is reached, CO-induced Rh particle disintegration occurs and the pre-exponential factor decreases due to the formation of inactive single atoms. When the initial average particle size is small, disintegration occurs at higher temperatures because the particles are not stable, due to their high surface energy and the formation of Rh(CO)$_2$ single atom complexes is more favorable—the adsorbate/Rh single atom, Rh(CO)$_2$, free energy is lower than that of CO bound to the Rh nanoparticle structure.[42] At larger particle sizes, the temperature has to be lower for CO-induced disintegration to occur because the larger particles are more stable.

In characterizing the more traditional sintering process, the cohesive energy of a small particle is weaker than that of a large particle, which means that a lower temperature would lead to sintering for small nanoparticles compared to that required for larger particles. The trend with particle size via the adsorbate-induced disintegration observed here is opposite of the traditional sintering trend.

Since this CO adsorbate-induced process is reversible, one can also consider the nanoparticles-single atoms dynamics

from low to high temperature. As temperature increases, for these CO-induced changes, bigger particles with their greater cohesive energy remain intact. Smaller particles will not form until higher temperature since CO-induced nanoparticle disintegration free energy of the smaller particles more easily overcomes the lesser cohesive energy needed to maintain their agglomerated state. This is consistent with theoretical studies[42] where first-principle calculations on Rh/TiO$_2$ showed that the driving force that leads to the particle disintegration increases with a decrease in particle size as the free energy of disintegration shows substantially more exergonic values.

In Situ CO + O$_2$ DRIFTS

In order to further investigate the structural dynamics occurring during the reaction, DRIFTS spectra were collected while exposing the 0.1%Rh/Al$_2$O$_3$ H$_2$-700 °C sample, characterized by a 1.6 nm particle size, to a CO and O$_2$ mixture with CO/O$_2$ = 0.9, a similar ratio used in the kinetic experiments described above. The spectra collected in the temperature range between 220 and 300 °C are shown in Figure 4. All the spectra were normalized by the intensity of
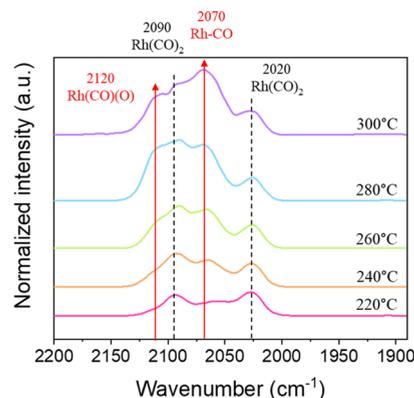
Figure 4. DRIFTS spectra of 0.1%Rh/Al$_2$O$_3$ H$_2$-700 °C during CO oxidation at 220 (lower spectrum), 240, 260, 280, and 300 °C (uppermost spectrum). CO = 8400 ppm; O$_2$ = 9250 ppm. The catalyst was first exposed to 1% O$_2$ at 500 °C for 30 min, followed by He purge for 10 min and 5% H$_2$ at 500 °C for 30 min. The spectra were normalized by the intensity of the peak at 2026 cm^{-1}, after applying the gas phase subtraction.

the asymmetric Rh *gem*-dicarbonyl peak, centered at ~2020 cm^{-1}. The spectra contain four peaks: 2070 cm^{-1}, assigned to the linear-bound CO on Rh^0, 2090 and 2026 cm^{-1}, corresponding to the symmetric and asymmetric *gem*-dicarbonyl species, respectively, and 2120 cm^{-1}, corresponding to Rh(CO)(O),[75] previously identified as a precursor to CO$_2$ on a Rh particle.[59,74] Overall, it is evident that with a decrease in temperature, the peak assigned to CO bound to the Rh nanoparticle decreased in intensity, while the relative intensities of the single atom features increased, providing additional evidence that CO induces particle disintegration with decreasing temperature.

To evaluate relative changes in the sites, the features in this region of each spectrum were deconvoluted and the areas under each peak were integrated. See Figure S8 and Section 6 of the Supporting Information deconvolution examples. Figure 5 shows the peak area ratios for the symmetric *gem*-dicarbonyls, indicated as 2090/2026, and the linear CO−Rh, indicated as 2070/2026. The ratio of the area of the two *gem*-dicarbonyl species is equal to 1, consistent with findings in the
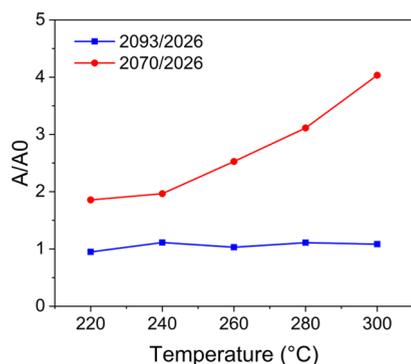
Figure 5. Normalized areas of symmetric and asymmetric *gem*-dicarbonyl features (2090/2026) and linear Rh−CO nanoparticle and asymmetric *gem*-dicarbonyl species (2070/2026) for each temperature investigated in the range between 220 and 300 °C.

Figure 6. DRIFTS spectra during CO + O$_2$ exposure at 260 °C on 0.1%Rh/Al$_2$O$_3$ H$_2$-700 °C. CO = 8400 ppm; O$_2$ = 2000, 4200, 6250, or 9250 ppm. The spectra were normalized by the highest intensity peak for comparison.

literature,[30] and this ratio remains 1 throughout the experiment, within the temperature range studied here. The ratios between the nanoparticle and the asymmetric *gem*-dicarbonyl are similar at 220 and 240 °C but increase with a further increase in temperature. In comparing the transition temperatures shown here and that in Figure 3, they are similar—the 0.1%Rh/Al$_2$O$_3$ H$_2$-700 °C sample is characterized by an average initial particle size of 1.6 nm and its *T change* during the CO oxidation kinetic study was 260 °C. The normalized Rh−CO area at 300 °C is 2-fold the initial area at 220−240 °C. These results are consistent with our kinetic data and provide additional evidence that the fractions of Rh particles and single atoms are changing during CO oxidation, and therefore, the fraction of active sites increases with an increase in temperature.

Effect of O$_2$ on Rh Speciation

The single atoms−nanoparticle interconversion during CO oxidation was observed only under conditions with an excess of oxygen, relative to stoichiometric CO oxidation. In fact, CO oxidation performed under oxygen-deficient and stoichiometric conditions showed a continuously linear Arrhenius plot, resulting in an activation energy of 110 kJ/mol. This suggests that oxygen enhances the oxidative process of CO-induced nanoparticle disruption. The effect of O$_2$ amount during CO adsorption/oxidation on 0.1% Rh/Al$_2$O$_3$ H$_2$-700 °C was investigated spectroscopically at 260 °C, which based on the results shown in Figure 3 is the single atom−nanoparticle transition region for this sample. The following concentrations were investigated: 2000, 4200, 6500, and 9250 ppm. The spectra in Figure 6 show that under stoichiometric conditions and conditions where there is excess CO, Rh speciation is not altered, as the only features present were the linear- and bridge-bound CO on Rh particles. However, when the O$_2$ concentration increased past the stoichiometric point, there was an increase in single atom fraction. Simultaneously, as shown in Figure S9, as the O$_2$ concentration increased, the negative feature in the 3600−3800 cm^{-1} OH region became more pronounced, suggesting that the OH groups on the Al$_2$O$_3$ surface were consumed. The increase in single atom formation and depletion of the OH groups with an increase in O$_2$ concentration is consistent with previous reports which postulated that the OH groups are involved in the Rh nanoparticle dispersion.[24,76,77] These spectra indicate that oxygen favors the CO-induced oxidative disruption of Rh nanoparticles (Rh^0) into Rh^I(CO)$_2$. This is consistent with our
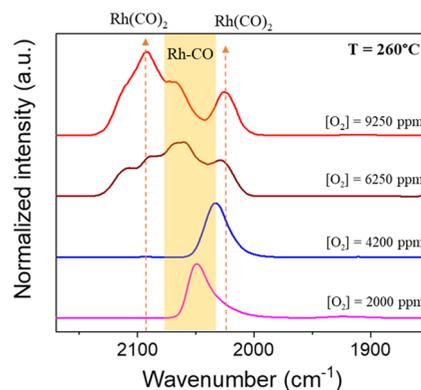
kinetic experiments performed under similar conditions where a deviation from the typical linear regime of an Arrhenius plot was not detected unless there was an excess of oxygen.

Bridging the Spectroscopic and Kinetic Data

As mentioned above, the Arrhenius plots in Figure 2 show the CO$_2$ formation rates expressed in mol/s due to the challenge in counting Rh active sites with their dynamics during the reaction. However, a quantitative interpretation of the spectroscopic data showed that at high temperature, the fraction of CO bound to the surface of the nanoparticles, proportional to the number of active sites, is 2 times higher than the fraction at low temperature. This information can be, and here was, used to normalize the reaction rates and obtain the CO oxidation turnover frequency.

The black squares in Figure 7 display the CO oxidation rate measured at high and low temperature on 0.1%Rh/Al$_2$O$_3$ H$_2$-700 °C, normalized by the amount of surface Rh sites calculated via H$_2$ chemisorption. As previously shown, from the linear fitting derived from the low and high temperature, the activation energies are similar and equal to 100−110 kJ/mol, but the pre-exponential factors are different depending on
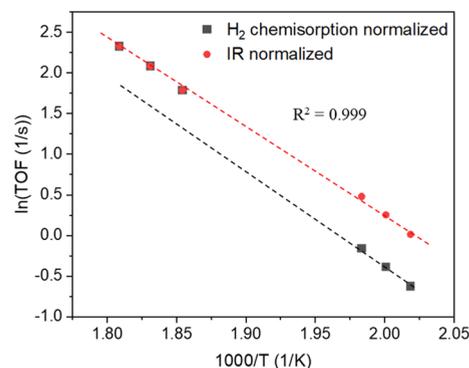
Figure 7. Normalized CO oxidation rates obtained on 0.1%Rh/Al$_2$O$_3$ H$_2$-700 °C. CO = 8400 ppm O$_2$ = 9250 ppm; total flowrate = 750 sccm. The catalyst was pre-reduced in 5% H$_2$ at 500 °C for 30 min. The black squares represent the reaction rates normalized by the number of Rh surface sites obtained from the H$_2$ chemisorption measurement and the red circles are the reaction rates normalized by the number of Rh surface sites obtained from the H$_2$ chemisorption at high temperature and the half that amount at low temperature based on the changes observed in the DRIFTS spectra.

the temperature region used. However, based on the DRIFTS results, the low-temperature regime has more single atoms and less particles, with a factor of 2 calculated when comparing relative peak intensities at 220−300 °C. We can therefore renormalize the pre-exponential factor by dividing the amount of Rh surface atoms obtained from H_2 chemisorption by 2 and use this quantity to normalize the rate measurements in the low-temperature regime. The red circles display the rate measurements normalized by two different active Rh amounts at low and high temperature. The resulting line fitting the red squares still gives an activation energy of 100 kJ/mol, consistent with our previous measurements.

This combined in situ spectroscopy and kinetic measurement method allows the quantification of the extent of particle disintegration and active site loss. The estimation of the active sites at all temperatures during the reaction allows the calculation a true turn over frequency that otherwise was not possible with just the reactor-based approach and ex situ active site measurements, which do not track the dynamics of nanoparticle−single atom interconversion.

CONCLUSIONS

CO oxidation structure insensitivity is an important tool that can be, and has been, used to identify and estimate the number of catalytically active sites. In this study, a combination of IR spectroscopy and CO oxidation kinetics was used to track the structural changes occurring on Rh/Al_2O_3 catalysts. We showed that the ability of CO to break Rh nanoparticles reduces the number of active sites during CO oxidation and the temperature where this occurs depends on the Rh particle size. With decreasing temperature, smaller particles broke apart to single atoms first, and the temperature required to break the particles decreased with increasing particle size up to 5 nm, after which the catalysts showed similar behavior. While H_2O does not affect the temperature at which the structural dynamics occur during the reaction, O_2 present in excess of the stoichiometric amount enhances CO-induced particle dispersion into single atoms. Spectroscopic studies were consistent with this behavior in the presence of excess O_2. Rh nanoparticle features were more intense at higher temperature compared to the IR features associated with single atoms, while at low temperature, the opposite was observed, implying that Rh nanoparticles were broken into single atoms at low temperature. In addition, semi-quantitative analysis of the DRIFTS spectra was consistent with the kinetic experiments, demonstrating that at low temperature only half of the original number of Rh active sites are present on the catalyst surface, compared to that at high temperature. Combining the relative changes in the DRIFTS spectra with the reactor-based kinetic experiments allowed the turnover frequency to be calculated on an exposed surface Rh basis.

ASSOCIATED CONTENT

Ⓢ Supporting Information

The Supporting Information is available free of charge at https://pubs.acs.org/doi/10.1021/jacsau.2c00595.

> H_2 chemisorption results, cordierite CO oxidation activity, CO oxidation Arrhenius plots, with and without H_2O, deconvolution of IR spectra examples, and mass and heat transfer calculations (PDF)

AUTHOR INFORMATION

Corresponding Author

William Epling − *Department of Chemical Engineering, University of Virginia, Charlottesville, Virginia 22903, United States;* ⓞ orcid.org/0000-0003-3421-101X; Email: wse2t@virginia.edu

Authors

Silvia Marino − *Department of Chemical Engineering, University of Virginia, Charlottesville, Virginia 22903, United States*

Lai Wei − *Department of Chemical Engineering, University of Virginia, Charlottesville, Virginia 22903, United States;* ⓞ orcid.org/0000-0003-3035-2851

Marina Cortes-Reyes − *Department of Chemical Engineering, University of Virginia, Charlottesville, Virginia 22903, United States;* ⓞ orcid.org/0000-0002-7314-3673

Yisun Cheng − *Research and Advanced Engineering, Ford Motor Company, Dearborn, Michigan 48124, United States*

Paul Laing − *Research and Advanced Engineering, Ford Motor Company, Dearborn, Michigan 48124, United States*

Giovanni Cavataio − *Research and Advanced Engineering, Ford Motor Company, Dearborn, Michigan 48124, United States*

Christopher Paolucci − *Department of Chemical Engineering, University of Virginia, Charlottesville, Virginia 22903, United States;* ⓞ orcid.org/0000-0002-4506-9306

Complete contact information is available at:
https://pubs.acs.org/10.1021/jacsau.2c00595

Author Contributions

CRediT: **Silvia Marino** conceptualization, data curation, formal analysis, methodology, writing-original draft, writing-review & editing; **Lai Wei** formal analysis.

Notes

The authors declare no competing financial interest.

REFERENCES

(1) Vogt, C.; Meirer, F.; Monai, M.; Groeneveld, E.; Ferri, D.; van Santen, R. A.; Nachtegaal, M.; Unocic, R. R.; Frenkel, A. I.; Weckhuysen, B. M. Dynamic Restructuring of Supported Metal Nanoparticles and Its Implications for Structure Insensitive Catalysis. *Nat. Commun.* **2021**, *12*, 7096.

(2) Batteas, J. D.; Dunphy, J. C.; Somorjai, G. A.; Salmeron, M. Coadsorbate Induced Reconstruction of a Stepped Pt(111) Surface by Sulfur and CO: A Novel Surface Restructuring Mechanism Observed by Scanning Tunneling Microscopy. *Phys. Rev. Lett.* **1996**, *77*, 534−537.

(3) Somorjai, G. A. The Experimental Evidence of the Role of Surface Restructuring during Catalytic Reactions. *Catal. Lett.* **1992**, *12*, 17−34.

(4) Yan, G.; Tang, Y.; Li, Y.; Li, Y.; Nguyen, L.; Sakata, T.; Higashi, K.; Tao, F. F.; Sautet, P. Reaction Product-Driven Restructuring and Assisted Stabilization of a Highly Dispersed Rh-on-Ceria Catalyst. *Nat. Catal.* **2022**, *5*, 119−127.

(5) Eren, B.; Zherebetskyy, D.; Patera, L. L.; Wu, C. H.; Bluhm, H.; Africh, C.; Wang, L. W.; Somorjai, G. A.; Salmeron, M. Activation of

Cu(111) Surface by Decomposition into Nanoclusters Driven by CO Adsorption. *Science* **2016**, *351*, 475−478.

(6) Felvey, N.; Guo, J.; Rana, R.; Xu, L.; Bare, S. R.; Gates, B. C.; Katz, A.; Kulkarni, A. R.; Runnebaum, R. C.; Kronawitter, C. X. Interconversion of Atomically Dispersed Platinum Cations and Platinum Clusters in Zeolite ZSM-5 and Formation of Platinum Gem-Dicarbonyls. *J. Am. Chem. Soc.* **2022**, *144*, 13874.

(7) Matsubu, J. C.; Yang, V. N.; Christopher, P. Isolated Metal Active Site Concentration and Stability Control Catalytic CO_2 Reduction Selectivity. *J. Am. Chem. Soc.* **2015**, *137*, 3076−3084.

(8) Asokan, C.; Yang, Y.; Dang, A.; Getsoian, A. "B.".; Christopher, P. Low-Temperature Ammonia Production during NO Reduction by CO Is Due to Atomically Dispersed Rhodium Active Sites. *ACS Catal.* **2020**, *10*, 5217−5222.

(9) Theis, J. R.; Ura, J. A. Assessment of Zeolite-Based Low Temperature NOx Adsorbers: Effect of Reductants during Multiple Sequential Cold Starts. *Catal. Today* **2021**, *360*, 340−349.

(10) Gu, Y.; Zelinsky, R. P.; Chen, Y.; Epling, W. S. Investigation of an Irreversible NOx Storage Degradation Mode on a Pd/BEA Passive NOx Adsorber. *Appl. Catal., B* **2019**, *258*, 118032.

(11) Solymosi, F.; Novák, E.; Molnar, A. Infrared Spectroscopic Study on CO-Induced Structural Changes of Iridium on an Alumina Support. *J. Phys. Chem.* **1990**, *94*, 7250−7255.

(12) Newton, M. A.; Belver-Coldeira, C.; Martínez-Arias, A.; Fernández-García, M. Dynamic in Situ Observation of Rapid Size and Shape Change of Supported Pd Nanoparticles during CO/NO Cycling. *Nat. Mater.* **2007**, *6*, 528−532.

(13) Moliner, M.; Gabay, J. E.; Kliewer, C. E.; Carr, R. T.; Guzman, J.; Casty, G. L.; Serna, P.; Corma, A. Reversible Transformation of Pt Nanoparticles into Single Atoms inside High-Silica Chabazite Zeolite. *J. Am. Chem. Soc.* **2016**, *138*, 15743−15750.

(14) Lardinois, T. M.; Mandal, K.; Yadav, V.; Wijerathne, A.; Bolton, B. K.; Lippie, H.; Li, C. W.; Paolucci, C.; Gounder, R. Kinetic and Thermodynamic Factors Influencing Palladium Nanoparticle Redispersion into Mononuclear Pd(II) Cations in Zeolite Supports. *J. Phys. Chem. C* **2022**, *126*, 8337−8353.

(15) Kale, M. J.; Christopher, P. Utilizing Quantitative in Situ FTIR Spectroscopy to Identify Well-Coordinated Pt Atoms as the Active Site for CO Oxidation on Al_2O_3-Supported Pt Catalysts. *ACS Catal.* **2016**, *6*, 5599−5609.

(16) Chee, S. W.; Arce-Ramos, J. M.; Li, W.; Genest, A.; Mirsaidov, U. Structural Changes in Noble Metal Nanoparticles during CO Oxidation and Their Impact on Catalyst Activity. *Nat. Commun.* **20202020**, *11*, 1−9.

(17) Gao, F.; Walter, E. D.; Kollar, M.; Wang, Y.; Szanyi, J.; Peden, C. H. F. Understanding Ammonia Selective Catalytic Reduction Kinetics over Cu/SSZ-13 from Motion of the Cu Ions. *J. Catal.* **2014**, *319*, 1−14.

(18) Paolucci, C.; Khurana, I.; Parekh, A. A.; Li, S.; Shih, A. J.; Li, H.; Di Iorio, J. R.; Albarracin-Caballero, J. D.; Yezerets, A.; Miller, J. T.; Delgass, W. N.; Ribeiro, F. H.; Schneider, W. F.; Gounder, R. Dynamic Multinuclear Sites Formed by Mobilized Copper Ions in NOx Selective Catalytic Reduction. *Science* **2017**, *357*, 898−903.

(19) Goodman, E. D.; Johnston-Peck, A. C.; Dietze, E. M.; Wrasman, C. J.; Hoffman, A. S.; Abild-Pedersen, F.; Bare, S. R.; Plessow, P. N.; Cargnello, M. Catalyst Deactivation via Decomposition into Single Atoms and the Role of Metal Loading. *Nat. Catal.* **2019**, *2*, 748−755.

(20) Basu, P. B.; Panayotov, J. T.; Yates, J. T. Rhodium-Carbon Monoxide Surface Chemistry: The Involvement of Surface Hydroxyl Groups on A12O3 and SiO2Supports. *J. Am. Chem. Soc.* **1988**, *110*, 2074−2081.

(21) Yates, J. T.; Duncan, T. M.; Vaughan, R. W. Infrared Spectroscopic Study of Activated Surface Processes: CO Chemisorption on Supported Rh. *J. Chem. Phys.* **1979**, *71*, 3908−3915.

(22) Bergeret, G.; Gallezot, P.; Gelin, P.; Ben Taarit, Y.; Lefebvre, F.; Naccache, C.; Shannon, R. D. CO-Induced Disintegration of Rhodium Aggregates Supported in Zeolites: In Situ Synthesis of Rhodium Carbonyl Clusters. *J. Catal.* **1987**, *104*, 279−287.

(23) Zaki, M. I.; Kunzmann, G.; Gates, B. C.; Knoezinger, H. Highly Dispersed Rhodium on Alumina Catalysts: Influence of the Atmosphere on the State and Dispersion of Rhodium. *J. Phys. Chem.* **1987**, *91*, 1486−1493.

(24) Basu, P.; Panayotov, D.; Yates, J. T. Spectroscopic Evidence for the Involvement of OH Groups in the Formation of $Rh^I(CO)_2$ on Metal Oxide Supports. *J. Phys. Chem.* **1987**, *91*, 3133−3136.

(25) Cavanagh, R. R.; Yates, J. T. Site Distribution Studies of Rh Supported on Al2O3 - An Infrared Study of Chemisorbed CO. *J. Chem. Phys.* **1981**, *74*, 4150−4155.

(26) Chen, J. G.; Colaianni, M. L.; Chen, P. J.; Yates, J. T.; Fisher, G. B. Thermal Behavior of a Rh/Al_2O_3 Model Catalyst: Disappearance of Surface Rh upon Heating. *J. Phys. Chem.* **1990**, *94*, 5059−5062.

(27) Duncan, T. M.; Yates, J. T.; Vaughan, R. W. A ^{13}C NMR Study of the Adsorbed States of CO on Rh Dispersed on Al2O3. *J. Chem. Phys.* **1980**, *73*, 975−985.

(28) Kiss, J. T.; Gonzalez, R. D. Catalytic Oxidation of Carbon Monoxide over Rh/SiO_2. An in Situ Infrared and Kinetic Study. *J. Phys. Chem.* **1984**, *88*, 898−904.

(29) Wang, H. P.; Yates, J. T. Spectroscopic Study of the Interconversion of Chemisorbed Surface Species: The Reaction $Rh^I(CO)_2 + CO \rightarrow Rh^I(CO)_3$. *J. Catal.* **1984**, *89*, 79−92.

(30) Yates, J. T.; Duncan, T. M.; Worley, S. D.; Vaughan, R. W. Infrared Spectra of Chemisorbed CO on Rh. *J. Chem. Phys.* **1979**, *70*, 1219−1224.

(31) Thiel, P. A.; Williams, E. D.; Yates, J. T.; Weinberg, W. H. The Chemisorption of CO on Rh(111). *Surf. Sci.* **1979**, *84*, 54−64.

(32) Wang, H. P.; Yates, J. T. Infrared Spectroscopic Study of N_2 Chemisorption on Rhodium Surfaces. *J. Phys. Chem.* **1984**, *88*, 852−856.

(33) Yates, J. T.; Kolasinski, K. Infrared Spectroscopic Investigation of the Rhodium Gem-Dicarbonyl Surface Species. *J. Chem. Phys.* **1983**, *79*, 1026−1030.

(34) Goellner, J. F.; Gates, B. C.; Vayssilov, G. N.; Rösch, N. Structure and Bonding of a Site-Isolated Transition Metal Complex: Rhodium Dicarbonyl in Highly Dealuminated Zeolite Y. *J. Am. Chem. Soc.* **2000**, *122*, 8056−8066.

(35) Van't Blik, H. F. J.; Van Zon, J. B. A. D.; Huizinga, T.; Vis, J. C.; Koningsberger, D. C.; Prins, R. Structure of Rhodium in an Ultradispersed Rh/Al_2O_3 Catalyst as Studied by EXAFS and Other Techniques. *J. Am. Chem. Soc.* **1985**, *16*, 3139−3147.

(36) Van't Blik, H. F. J.; Van Zon, J. B. A. D.; Koningsberger, D. C.; Prins, R. EXAFS Determination of the Change in the Structure of Rhodium in Highly Dispersed $Rh/\gamma-Al_2O_3$ Catalysts after CO and/or H_2 Adsorption at Different Temperatures. *J. Mol. Catal.* **1984**, *25*, 379−396.

(37) Dohmae, K.; Nagai, Y.; Tanabe, T.; Suzuki, A.; Inada, Y.; Nomura, M. Real-Time XAFS Analysis of Rh/Alumina Catalyst. *Surf. Interface Anal.* **2008**, *40*, 1751−1754.

(38) Berkó, A.; Solymosi, F. Adsorption-Induced Structural Changes of Rh Supported by TiO2(110)-(1×2): An STM Study. *J. Catal.* **1999**, *183*, 91−101.

(39) Matsubu, J. C.; Zhang, S.; DeRita, L.; Marinkovic, N. S.; Chen, J. G.; Graham, G. W.; Pan, X.; Christopher, P. Adsorbate-Mediated Strong Metal-Support Interactions in Oxide-Supported Rh Catalysts. *Nat. Chem.* **2017**, *9*, 120−127.

(40) Robbins, J. L. Rhodium Dicarbonyl Sites on Alumina Surface. Preparation and Characterization of a Model System. *J. Phys. Chem. C* **1986**, *90*, 3381−3386.

(41) Iordan, R.; Zaki, C.; Kappenstein, K.; Géron, A.; Zaki, M. I.; Kappenstein, C.; Géron, C.; Al, B.; Al, K. XPS and in Situ IR Spectroscopic Studies of $CO/Rh/Al_2O_3$ and $CO/Rh/K−Al_2O_3$ at High Temperatures: Probing the Impact of the Potassium Functionalization of the Support. *Phys. Chem. Chem. Phys.* **2003**, *5*, 1708−1715.

(42) Ouyang, R.; Liu, J. X.; Li, W. X. Atomistic Theory of Ostwald Ripening and Disintegration of Supported Metal Particles under Reaction Conditions. *J. Am. Chem. Soc.* **2013**, *135*, 1760−1771.

(43) Goldsmith, B. R.; Sanderson, E. D.; Ouyang, R.; Li, W. X. CO- and NO-Induced Disintegration and Redispersion of Three-Way Catalysts Rhodium, Palladium, and Platinum: An Ab Initio Thermodynamics Study. *J. Phys. Chem. C* **2014**, *118*, 9588−9597.

(44) Van't Blik, H. F. J.; Van Zon, J. B. A. D.; Huizinga, T.; Vis, J. C.; Koningsberger, D. C.; Prins, R. An Extended X-Ray Absorptlon Flne Structure Spectroscopy Study of a Highly Dispersed Rh/Al$_2$O$_3$ Catalyst: The Influence of CO Chemisorption on the Topology of Rhodium. *J. Phys. Chem.* **1983**, *87*, 2264−2267.

(45) Van't Blik, H. F. J.; Van Zon, T.; Huizinga, J. B. A. D.; Vis, J. C.; Koningsberger, D. C.; Prins, R. Structure of Rhodium in an Ultradispersed Rh/Al$_2$O$_3$ Catalyst as Studied by EXAFS and Other Techniques. *J. Am. Chem. Soc.* **1985**, *107*, 3139−3147.

(46) Rainer, D. R.; Koranne, M.; Vesecky, S. M.; Goodman, D. W. CO + O$_2$ and CO + NO Reactions over Pd/Al$_2$O$_3$ Catalysts. *J. Phys. Chem. B* **1997**, *101*, 10769−10774.

(47) Cargnello, M.; Doan-Nguyen, V. V. T.; Gordon, T. R.; Diaz, R. E.; Stach, E. A.; Gorte, R. J.; Fornasiero, P.; Murray, C. B. Control of Metal Nanocrystal Size Reveals Metal-Support Interface Role for Ceria Catalysts. *Science* **2013**, *341*, 771−773.

(48) Freund, H. J.; Meijer, G.; Scheffler, M.; Schlögl, R.; Wolf, M. CO Oxidation as a Prototypical Reaction for Heterogeneous Processes. *Angew. Chem., Int. Ed.* **2011**, *50*, 10064−10094.

(49) Chee, S. W.; Arce-Ramos, J. M.; Li, W.; Genest, A.; Mirsaidov, U. Structural Changes in Noble Metal Nanoparticles during CO Oxidation and Their Impact on Catalyst Activity. *Nat. Commun.* **2020**, *11*, 2133.

(50) Hepburn, J. S.; Dobson, D. A.; Hubbard, C. P.; Otto, K. The Pulse Flame Combustor Revisited. *SAE Tech. Pap. Ser.* **1996**, *105*, 2296−2331.

(51) Farrauto, R. J.; Deeba, M.; Alerasool, S. Gasoline Automobile Catalysis and Its Historical Journey to Cleaner Air. *Nat. Catal.* **2019**, *2*, 603−613.

(52) Weisz, P. B.; Prater, C. D. Interpretation of Measurements in Experimental Catalysis. *Adv. Catal.* **1954**, *6*, 143−196.

(53) Mears, D. E. Diagnostic Criteria for Heat Transport Limitations in Fixed Bed Reactors. *J. Catal.* **1971**, *20*, 127−131.

(54) Mears, D. E. Tests for Transport Limitations in Experimental Catalytic Reactors. *Ind. Eng. Chem. Process Des. Dev.* **1971**, *10*, 541−547.

(55) Yates, D. J. C.; Murrell, L. L.; Prestridge, E. B. Ultradispersed Rhodium Rafts: Their Existence and Topology. *J. Catal.* **1979**, *57*, 41−63.

(56) Yates, D. J. C.; Sinfelt, J. H. The Catalytic Activity of Rhodium in Relation to Its State of Dispersion. *J. Catal.* **1967**, *8*, 348−358.

(57) Asokan, C.; DeRita, L.; Christopher, P. Using Probe Molecule FTIR Spectroscopy to Identify and Characterize Pt-Group Metal Based Single Atom Catalysts. *Chin. J. Catal.* **2017**, *38*, 1473−1480.

(58) Asokan, C.; Thang, H. V.; Pacchioni, G.; Christopher, P. Reductant Composition Influences the Coordination of Atomically Dispersed Rh on Anatase TiO$_2$. *Catal. Sci. Technol.* **2020**, *10*, 1597−1601.

(59) Rice, C. A.; Worley, S. D.; Curtis, C. W.; Guin, J. A.; Tarrer, A. R. The Oxidation State of Dispersed Rh on Al$_2$O$_3$. *J. Chem. Phys.* **1981**, *74*, 6487−6497.

(60) Tang, Y.; Asokan, C.; Xu, M.; Graham, G. W.; Pan, X.; Christopher, P.; Li, J.; Sautet, P. Rh Single Atoms on TiO$_2$ Dynamically Respond to Reaction Conditions by Adapting Their Site. *Nat. Commun.* **2019**, *10*, 1−10.

(61) Szanyi, J.; Goodman, D. W. CO Oxidation on Palladium. 1. A Combined Kinetic-Infrared Reflection Absorption Spectroscopic Study of Pd(100). *J. Phys. Chem.* **1994**, *98*, 2972−2977.

(62) Song, J.; Yang, Y.; Liu, S.; Li, L.; Yu, N.; Fan, Y.; Chen, Z.; Kuai, L.; Geng, B. Dispersion and Support Dictated Properties and Activities of Pt/Metal Oxide Catalysts in Heterogeneous CO Oxidation. *Nano Res.* **2021**, *14*, 4841−4847.

(63) Farber, R. G.; Turano, M. E.; Killelea, D. R. Identification of Surface Sites for Low-Temperature Heterogeneously Catalyzed CO Oxidation on Rh(111). *ACS Catal.* **2018**, *8*, 11483−11490.

(64) Gustafson, J.; Balmes, O.; Zhang, C.; Shipilin, M.; Schaefer, A.; Hagman, B.; Merte, L. R.; Martin, N. M.; Carlsson, P.-A.; Jankowski, M.; Crumlin, E. J.; Lundgren, E. The Role of Oxides in Catalytic CO Oxidation over Rhodium and Palladium. *ACS Catal.* **2018**, *8*, 4438−4445.

(65) Allian, A. D.; Takanabe, K.; Fujdala, K. L.; Hao, X.; Truex, T. J.; Cai, J.; Buda, C.; Neurock, M.; Iglesia, E. Chemisorption of CO and Mechanism of CO Oxidation on Supported Platinum Nanoclusters. *J. Am. Chem. Soc.* **2011**, *133*, 4498−4517.

(66) Gao, F.; Cai, Y.; Gath, K. K.; Wang, Y.; Chen, M. S.; Guo, Q. L.; Goodman, D. W. CO Oxidation on Pt-Group Metals from Ultrahigh Vacuum to Near Atmospheric Pressures. 1. Rhodium. *J. Phys. Chem. C* **2009**, *113*, 182−192.

(67) Gao, F.; Wang, Y.; Cai, Y.; Goodman, D. W. CO Oxidation on Pt-Group Metals from Ultrahigh Vacuum to Near Atmospheric Pressures . 2. Palladium and Platinum *J. Phys. Chem. C* **2009**, *113*(), 174−181. DOI: 10.1021/jp8077985.

(68) Engel, T.; Ertl, G. Elementary Steps in the Catalytic Oxidation of Carbon Monoxide on Platinum Metals. *Adv. Catal.* **1979**, *28*, 1−78.

(69) McClure, S. M.; Goodman, D. W. New Insights into Catalytic CO Oxidation on Pt-Group Metals at Elevated Pressures. *Chem. Phys. Lett.* **2009**, *469*, 1−13.

(70) Oh, S. H.; Eickel, C. C. Influence of Metal Particle Size and Support on the Catalytic Properties of Supported Rhodium: CO-O$_2$ and CO-NO Reactions. *J. Catal.* **1991**, *128*, 526−536.

(71) Peden, C. H. F.; Goodman, D. W.; Blair, D. S.; Berlowitz, P. J.; Fisher, G. B.; Oh, S. H. Kinetics of CO Oxidation by O$_2$ or NO on Rh(111) and Rh(100) Single Crystal. *J. Phys. Chem.* **1988**, *92*, 1563−1567.

(72) Oh, S. H.; Fisher, G. B.; Carpenter, J. E.; Goodman, D. W. Comparative Kinetic Studies of CO-O$_2$ and CO-NO Reactions over Single Crystal and Supported Rhodium Catalysts. *J. Catal.* **1986**, *100*, 360−376.

(73) Leung, L.-W. H.; Goodman, D. The Oxidation of Carbon Monoxide on Rh(100) Under Steady State Conditions: An FT-IR Study. *Catal. Lett.* **1990**, *5*, 353−359.

(74) Cavers, M.; Davidson, J. M.; Harkness, I. R.; Rees, L. V. C.; McDougall, G. S. Spectroscopic Identification of the Active Site for CO Oxidation on Rh/Al$_2$O$_3$ by Concentration Modulation in Situ DRIFTS. *J. Catal.* **1999**, *188*, 426−430.

(75) Wovchko, E. A.; Yates, J. T. Activation of O$_2$ on a Photochemically Generated Rh^I Site on an Al$_2$O$_3$ Surface: Low-Temperature O$_2$ Dissociation and CO Oxidation. *J. Am. Chem. Soc.* **1998**, *120*, 10523−10527.

(76) Solymosi, F.; Pasztor, M. An Infrared Study of the Influence of CO Chemisorption on the Topology of Supported Rhodium. *J. Phys. Chem.* **1985**, *89*, 4789−4793.

(77) Solymosi, F.; Pasztor, M. Infrared Study of the Effect of H$_2$ on CO-Induced Structural Changes in Supported Rh. *J. Phys. Chem.* **1986**, *90*, 5312−5317.